Research Square

Preprints are preliminary reports that have not undergone peer review.
They should not be considered conclusive, used to inform clinical practice,
or referenced by the media as validated information.

Edible Alginate Hydrogels Functionalized With Okara Proteins and Yerba Mate Polyphenols as Sustainable Scaffolds for Cultivated Meat

Carlos Henrique Colombo
Federal University of Santa Catarina
Ana Paula Zapelini Melo
University of California, Davis
Sarah Hope Assaf Furtado
Federal University of Santa Catarina
Giordana Demaman Arend
Federal University of Santa Catarina
Ana Paula Bastos
Embrapa Suínos e Aves
Katia Rezzadori
katia.rezzadori@ufsc.br

Federal University of Santa Catarina

Research Article

Keywords: Cellular agriculture, Circular economy, Food-grade biomaterials, Hydrogels, Okara, Plant-based scaffolds

Posted Date: June 4th, 2026

DOI: https://doi.org/10.21203/rs.3.rs-9782489/v1

License: This work is licensed under a Creative Commons Attribution 4.0 International License.
Read Full License

Additional Declarations: No competing interests reported.

EDIBLE ALGINATE HYDROGELS FUNCTIONALIZED WITH OKARA PROTEINS AND YERBA MATE POLYPHENOLS AS SUSTAINABLE SCAFFOLDS FOR CULTIVATED MEAT

Carlos Henrique Colombo[a], Ana Paula Zapelini de Melo[a,b], Sarah Hope Assaf Furtado[a], Giordana Demaman Arend[c], Ana Paula Bastos[d], Katia Rezzadori[a*]

[a]Department of Food Science and Technology, Agricultural Sciences Center, Federal University of Santa Catarina, 88034-001 Florianópolis, SC, Brazil.

[b]Department of Biological and Agricultural Engineering, University of California, Davis, 95618, Davis, California, United States.

[c]Department of Chemical and Food Engineering, Technological Center, Federal University of Santa Catarina, 88034-001 Florianopolis, SC, Brazil.

[d]Embrapa Suínos e Aves, Rodovia BR 153, Km 110, Concórdia, SC 89715-899, Brazil.

Orcid ID Carlos Henrique Colombo: 0000-0001-9709-9542

Orcid ID Ana Paula Zapelini de Melo: 0000-0002-4053-2277

Orcid ID Giordana Demaman Arend: 0000-0002-4889-7510

Orcid ID Ana Paula Bastos: 0000-0002-0873-1639

Orcid ID Katia Rezzadori: 0000-0002-5878-0711

**Corresponding author:*

Prof. Dr. Katia Rezzadori

Departamento de Ciência e Tecnologia de Alimentos, Centro de Ciências Agrárias, Universidade Federal de Santa Catarina, Avenida Ademar Gonzaga, 1346, 88034-001, Itacorubi, Florianópolis, SC, Brazil

E-mail address: katia.rezzadori@ufsc.br

Phone number: +55 48 988328463

ABSTRACT

Cultivated meat production requires edible, sustainable scaffolds that mimic the native extracellular matrix while supporting cell growth and differentiation. Although most scaffold studies rely on C2C12 murine cell lines, this study advances the field by developing and validating an animal-free scaffold platform using primary bovine myoblasts. Ca^{2+}-crosslinked alginate hydrogels were functionalized with okara powder (OKP) (1.5-5% w/v) and yerba mate polyphenols, representing a novel strategy for incorporating agro-industrial by-products into scaffolds for cellular agriculture. The hydrogels were produced via ionic gelation and characterized using scanning electron microscopy (SEM), porosity measurements, attenuated total reflectance Fourier transform infrared spectroscopy (ATR-FTIR), mechanical analyses (shear stress and compression), and simulated gastrointestinal digestion. Biocompatibility assays demonstrated that the scaffold containing 5% OKP significantly increased cell density, reaching 2.66×10^6 cells after 7 days and outperforming both the 2.5% OKP and control groups. In addition, the 5% OKP scaffold exhibited an interconnected microporous structure with 43% porosity, promoting deeper cell infiltration and improved adhesion of primary bovine myoblasts compared with the control alginate matrix. The incorporation of okara proteins and yerba mate polyphenols also contributed to the development of hydrophilic and bioactive scaffolds with potential to support cultivated meat applications. Overall, the results demonstrate the feasibility of valorizing okara and yerba mate as functional ingredients in edible scaffolds while supporting primary bovine myoblast growth, contributing to sustainable and circular bioeconomy strategies for cultivated meat production.

Keywords: Cellular agriculture; Circular economy; Food-grade biomaterials; Hydrogels; Okara; Plant-based scaffolds.

1. INTRODUCTION

Cultivated meat produced via animal cell culture has emerged as a promising alternative protein platform, with the potential to reduce reliance on conventional livestock systems, depending on process design and energy inputs (Goodwin, Aimutis, & Shirwaiker, 2024; Murugan et al., 2024). Despite recent advances in commercialization, key challenges remain regarding production costs, scalability, and the development of structured products with meat-like texture and sensory characteristics (Stout, Kaplan, & Flack, 2023). In this context, edible scaffolds play a central role by providing a three-dimensional microenvironment that supports cell attachment, proliferation, and differentiation while enabling efficient mass transfer and nutrient diffusion throughout the construct (Gomez & Boyle, 2023; Alam et al., 2024).

Beyond providing structural support for cell growth, edible scaffolds for cultivated meat should also enhance the final product's nutritional and functional quality. Since these biomaterials are expected to remain integrated into the edible matrix, their digestibility, bioaccessibility, and potential contribution to nutrient delivery become important design criteria. Consequently, the development of food-grade scaffolds has progressively shifted from a purely tissue-engineering perspective toward multifunctional systems that combine structural performance, biocompatibility, and nutritional value (Bomkamp et al., 2021; Mariano Jr. et al., 2025). Recent studies have highlighted the importance of incorporating food safety evaluation, digestibility assessment, and functionality analyses when designing edible scaffolds for cultivated meat applications, reinforcing the need for biomaterials that are not only suitable for cell culture but also compatible with food consumption requirements (Mariano Jr. et al., 2025). Consequently, hydrogel-based edible scaffolds have attracted increasing attention for their ability to simultaneously provide structural support and food functionality.

Hydrogel formulations based on alginate, gelatin, collagen, chitosan, and plant proteins have been explored to improve cell adhesion, porosity, and mechanical performance for cultivated meat applications. Recent studies have also incorporated bioactive compounds and polyphenols to enhance scaffold functionality and biocompatibility (Li et al., 2022; Chen et al., 2023; Park et al., 2024; Narayanan et al., 2025). Among food-grade hydrogel matrices, sodium alginate (SA) has received particular attention due to its mild gelation conditions, biocompatibility, and ability to form ionically crosslinked networks in the presence of divalent cations such as Ca^{2+} (Gombotz & Wee, 2012; Hecht & Srebnik, 2016). Nevertheless, alginate matrices generally exhibit limited cell-adhesive properties and relatively dense structures, which may restrict cell infiltration and hinder the formation of thicker constructs (Campbell, Stilhano, & Silva, 2018). Consequently, strategies capable of modifying the organization of alginate networks while simultaneously improving scaffold functionality remain necessary.

In this regard, incorporating agro-industrial coproducts rich in proteins and bioactive compounds represents a promising approach for developing multifunctional edible scaffolds. Okara, a by-product of soy processing, is rich in proteins and dietary fiber, and its protein fraction can interact with polysaccharides through electrostatic interactions and hydrogen bonding, potentially improving water retention, structural organization, and mechanical properties (Wu et al., 2024). Likewise, yerba mate (*Ilex paraguariensis*) is an important source of polyphenolic compounds that may interact with biopolymer matrices, influencing gel organization and stability while providing antioxidant functionality (Cardozo et al., 2021; Chen et al., 2023; Ejiohuo et al., 2024). Furthermore, the use of these materials aligns with circular economy principles by promoting the valorization of

agro-industrial residues. Despite advances in edible hydrogel scaffolds, studies integrating protein-rich coproducts and polyphenol-rich ingredients into alginate-based systems for cultivated meat applications remain. The incorporation of okara-derived proteins and yerba mate polyphenols is expected to modulate interactions within the alginate network, potentially improving scaffold structure and functionality while promoting the valorization of agro-industrial residues.

Therefore, this study aimed to develop Ca^{2+}-crosslinked alginate hydrogels functionalized with okara-derived proteins and yerba mate polyphenols and to evaluate their physicochemical, structural, mechanical, antioxidant, and biological properties as edible scaffolds for cultivated meat applications.

2 MATERIALS AND METHODS

2.1 Materials and reagents

All reagents were of analytical grade and used as received. Hydrochloric acid, $ABTS^{+}$, Trolox, sodium carbonate, calcium chloride, ferric chloride hexahydrate, ethanol, formaldehyde, glutaraldehyde, isopropanol, 2,2-diphenyl-1-picrylhydrazyl (DPPH), Folin–Ciocalteu reagent, and penicillin–streptomycin–amphotericin (PSA) were purchased from Sigma-Aldrich (St. Louis, MO, USA). Dulbecco's Modified Eagle Medium (DMEM) and fetal bovine serum (FBS) were obtained from Cytiva HyClone (Logan, UT, USA). Fluorescent dyes and 3-(4,5-dimethylthiazol-2-yl)-2,5-diphenyltetrazolium bromide (MTT) were purchased from Thermo Fisher Scientific (USA). Molecular biology kits were obtained from Applied Biosystems (Foster City, CA, USA). The okara flour used in the scaffold formulations was prepared as described by Canaan et al. (2022). The yerba mate extract (2%) was produced following the procedure described by Layly et al. (2015), yielding a final phenolic composition of 1.77 ± 0.02 mg GAE/mL.

2.2 Edible scaffolds preparation

The scaffolds were prepared without animal-derived components, following methodologies previously described in the literature, with adaptations (Chen et al., 2023; Fang et al., 2025; Han et al., 2024), using a combination of okara, soy protein isolate (for structural support), yerba mate extract (polyphenols), sodium alginate (polysaccharide), calcium chloride as crosslinking agent, and glycerol as plasticizer.

A soy protein (SP) solution at 2.5% (w/v) was prepared in distilled water, heated in a water bath at 90 °C for 30 min, and subsequently cooled to room temperature. After cooling, glycerol (5% w/w) was added as a plasticizer. Okara powder (OKP) was then incorporated into the solution at different concentrations (0, 1.5, 2.5, 3.5, and 5% w/v), followed by homogenization for 5 min. Subsequently, the mixtures were combined with a 2% (v/v) sodium alginate (SA) solution at a 1:1 ratio and homogenized for 3 min using a vortex mixer.

In the next step, a 0.2% (w/v) yerba mate extract solution was added to the mixtures, followed by vortex homogenization for 3 min. The formulations were then dispensed into 24-well plates, with 1 mL of solution added to each well. Hydrogel crosslinking was induced by adding 58 µL of 2 M calcium chloride ($CaCl_2$) solution. After the addition of the crosslinking agent, the plates were manually agitated for 5 min and subsequently stored at −18 ± 2 °C for 16 h. Thereafter, the samples were transferred to an ultra-freezer (−80 °C) for 24 h as a preliminary step prior to the drying process.

Drying was carried out using a freeze-dryer (LT 3000 model, Terroni Fauvel, Brazil), with an initial stage of 2 h 30 min at −50 °C, followed by primary drying at a shelf temperature of 35 °C, for a total of 16 h of lyophilization. Figure 1 presents a graphical summary of the scaffold production method.

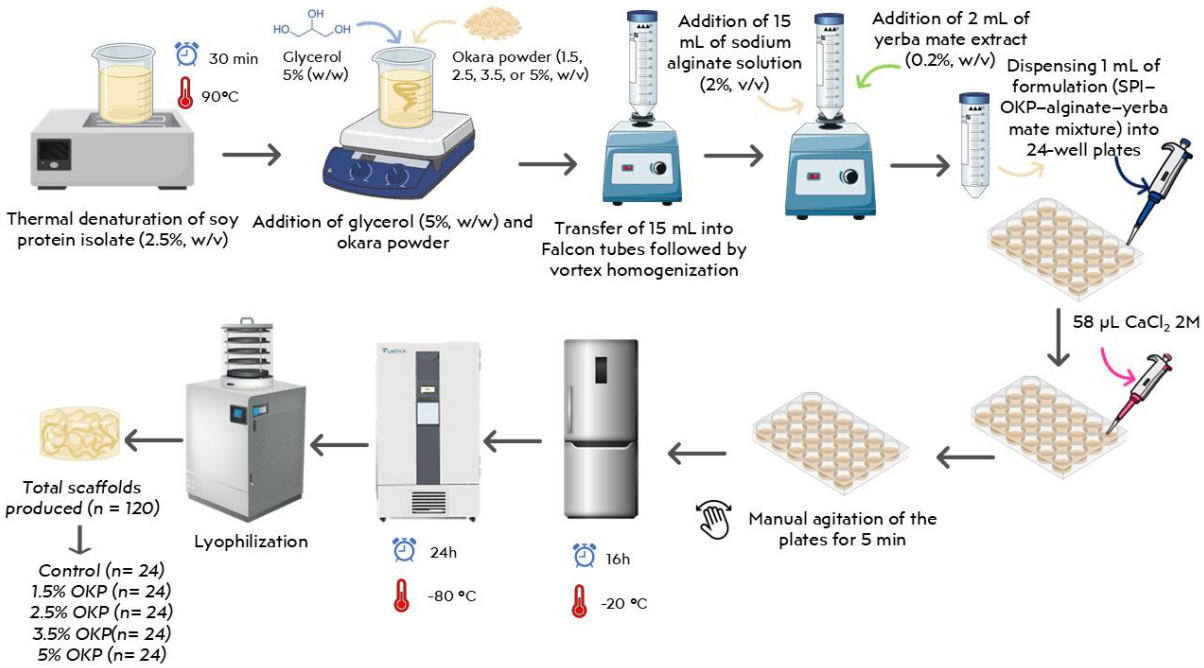


Fig. 1 Schematic overview of hydrogel preparation using okara, soy protein, sodium alginate, and calcium chloride for cultured meat scaffolds, highlighting the roles of bioactive components and ionic crosslinking in scaffold formation.

2.3 Scaffold characterization

2.3.1 Morphology characterization

Scaffolds were evaluated for diameter, thickness, microstructure, porosity, and average pore diameter. The diameter and thickness of the scaffolds were measured using a digital caliper (BOM-6502, BOMDER, São Paulo, Brazil). All measurements were performed in triplicate. The lyophilized scaffolds were mounted on aluminum stubs using carbon adhesive tape and sputter-coated with gold (EM SCD 500, Leica Microsystems, Germany) to ensure conductivity under vacuum conditions. The microstructure of the scaffolds was analyzed using a scanning electron microscope (SEM) (JEOL JSM-6390 LV, Tokyo, Japan) operating at an accelerating voltage of 10 kV and magnifications ranging from 50× to 1000×. Porosity analysis was performed according to the method described by Nokoorani et al. (2021). The porosity and average pore diameter of the scaffolds were determined using ImageJ software (version 1.54g).

2.3.2 Mechanical properties

The mechanical properties of the scaffolds were determined by shear force and compression tests using a TA.XT Plus texture analyzer (Stable Micro Systems Ltd., Godalming, United Kingdom). For the shear

force analysis, the equipment was fitted with a V-shaped cutting probe. The test conditions comprised pre-test, test, and post-test speeds of 1.0, 0.5, and 10.0 mm s^{-1}, respectively, with a cutting distance of 2 cm.

Compression tests were performed using the same texture analyzer equipped with a 5 kg load cell and a 26 mm cylindrical probe. Prior to analysis, the scaffolds were hydrated in phosphate-buffered saline (PBS) for 5 min and superficially dried with absorbent paper. The assays were conducted in simple compression mode at room temperature (25 ± 2 °C). Each sample was individually positioned at the center of the platform and aligned with the probe. The scaffolds were compressed at a rate of 0.5 mm s^{-1} until 10% deformation, as described by Fang et al. (2024). Measurements for each scaffold were performed in triplicate, and the maximum force (N) obtained using the Texture Exponent software was used as the parameter for comparison among the scaffolds.

2.3.3 Swelling ratio and biodegradation

The swelling ratio of the scaffolds was determined using methods described by Wang et al. (2024) and Chen et al. (2023). Lyophilized scaffolds (d = 10 mm, h = 3 mm) were immersed in phosphate-buffered saline (PBS, pH 7.4) at 37 °C and weighed at 4, 24, 48, and 72 h. The swelling ratio was calculated according to Equation (1):

$$Swelling\ ratio\ (\%) = \frac{(P2 - P1)}{P1} x\ 100 \quad (1)$$

where $P1$ is the initial weight of the scaffold before immersion (g), and $P2$ is the weight of the scaffold after immersion in PBS medium (g).

The biodegradation of the scaffolds was evaluated according to the method described by Wang et al. (2024), with modifications. Initially, the scaffolds were weighed to obtain the initial mass (PS) and subsequently immersed in phosphate-buffered saline (PBS, pH 7.4) at 37 °C for 72 h. After the incubation period, the samples were freeze-dried again using a lyophilizer (LT 3000, Terroni Fauvel, Brazil) and weighed to determine the final dry mass (PF). The biodegradation percentage was calculated according to Equation (2):

$$Biodegradation\ (\%) = \frac{(PS - PF)}{(PF)} x\ 100\ (2)$$

where PS is the initial scaffold weight (g), and PF is the dry weight of the degraded sample (g).

2.3.4 Chemical characterization

Attenuated Total Reflectance Fourier Transform Infrared Spectroscopy (ATR-FTIR) analyses were performed using a PerkinElmer Spectrum Two spectrometer (Massachusetts, USA) equipped with an ATR accessory containing a diamond crystal. The samples were directly placed on the crystal surface, and eight scans were collected for each measurement within the spectral range of 4000–650 cm^{-1} at a resolution of 4 cm^{-1}. The spectra obtained were corrected against the air background spectrum previously recorded with the empty crystal.

2.3.5 *In vitro* digestibility

The *in vitro* digestibility of the scaffolds was determined according to the method described by Verruck et al. (2015), with modifications. The assay simulated the human gastrointestinal digestion process through three sequential stages: oral, gastric, and intestinal phases. Initially, the reagent solutions were prepared, including sodium bicarbonate ($NaHCO_3$) solutions (1 and 0.1 M), calcium chloride ($CaCl_2$) solution (1 M), hydrochloric acid (HCl) solutions (1 and 0.1 M), and enzymatic solutions of α-amylase (100 $U \cdot mL^{-1}$), pepsin,

and pancreatin/bile mixture. All solutions were sterilized by filtration through 0.22 μm membranes. The digestion assay was conducted in a water bath under mechanical agitation at 37 ± 1 °C to simulate physiological gastrointestinal conditions.

During the oral phase, 1 g of sample was dispersed in 5 mL of distilled water, and the pH was adjusted to 6.9 using 0.1 M $NaHCO_3$ solution. Subsequently, 24 μL of α-amylase solution was added, and the mixture was agitated at 200 rpm for 1 min.

For the gastric phase, the pH was adjusted to 2.0 with 0.1 M HCl, followed by the addition of pepsin. The samples were maintained under agitation at 130 rpm and 37 °C.

During the intestinal phase, the pH was initially adjusted to 5.0 using 0.1 M $NaHCO_3$ solution, followed by the addition of 250 μL of pancreatin/bile solution to simulate duodenal conditions. The mixture was maintained under agitation at 45 rpm for 20 min. Subsequently, the pH was adjusted to 6.5 to simulate ileal conditions, and incubation was continued for an additional 90 min.

Polysaccharide release during the digestion process was determined according to the method described by Dubois et al. (1956), which involves reacting sugars with 5% (w/v) phenol and concentrated sulfuric acid to form a colored complex. After cooling, absorbance was measured at 490 nm using a UV–Vis spectrophotometer (mini-1240, Shimadzu, Tokyo, Japan), and quantification was performed using a glucose standard curve. The results were expressed as polysaccharide concentration (μg L^{-1}) throughout the different digestion phases.

Additionally, total phenolic compounds were quantified using the Folin–Ciocalteu method, as described by Singleton and Rossi (1965) and adapted by Arend et al. (2017). All reactions were conducted in the dark throughout the analytical procedure. Absorbance was measured at 750 nm using a UV–Vis spectrophotometer (mini-1240, Shimadzu, Tokyo, Japan), with distilled water used as a blank. The standard calibration curve was prepared using gallic acid solutions ranging from 200 to 800 μg mL^{-1}. The results were expressed as mg of gallic acid equivalents (GAE) mL^{-1} of extract.

Antioxidant activity was determined using the DPPH assay as described by Rufino et al. (2007). The antioxidant capacity was evaluated based on the reaction between the yerba mate extract and the methanolic DPPH solution. Absorbance readings were performed at 515 nm using a UV–Vis spectrophotometer (mini-1240, Shimadzu, Tokyo, Japan). Methanol was used as the blank solution. Trolox was used as the reference standard ($R^2 = 0.9861$), and the results were expressed as g of Trolox equivalents (TE) per liter.

2.4 Cell culture

2.4.1 Muscle cells and culture media

Mouse skeletal muscle C2C12 cells and primary bovine satellite cells (BSCs) were used as cellular models for muscle cell culture. The C2C12 cell line was used due to its high proliferative rate and well-established standardization protocols, making it an ideal model for initial biocompatibility screening prior to validation with primary bovine cells. Prior to the cell culture assays, the scaffolds were sterilized by autoclaving (15 min at 122 °C). After sterilization, each scaffold was subjected to a preconditioning process for 2 h in Dulbecco's Modified Eagle Medium (DMEM) supplemented with 10% fetal bovine serum (FBS) and penicillin/streptomycin at 37 °C in a humidified atmosphere containing 5% CO_2. This procedure aimed to promote the physicochemical equilibration of the material, facilitate nutrient diffusion into the matrix, and

remove possible soluble residues remaining from the fabrication process. The preconditioning medium was carefully removed immediately before cell seeding.

Immortalized mouse myoblasts (C2C12) were maintained in tissue culture flasks containing high-glucose Dulbecco's Modified Eagle Medium (DMEM; Gibco) supplemented with 10% fetal bovine serum (FBS; Gibco) and 1% penicillin–streptomycin (Gibco).

Primary bovine satellite cells were isolated from the semimembranosus muscle of an Angus bovine carcass. The excised tissues were immediately immersed in Dulbecco's phosphate-buffered saline without calcium and magnesium (DPBS −Ca/−Mg) supplemented with 1% Primocin. Subsequently, the tissues were washed three times with DPBS, trimmed to remove residual fat and connective tissue, and minced using sterile forceps and scissors.

For tissue digestion, the samples were transferred to a sterile centrifuge tube containing 60 mg of type I collagenase (Gibco) dissolved in 20 mL of DPBS. The solution was previously sterilized through a 0.22 μm membrane filter. The tube was incubated in a water bath at 37 °C for 1.5 h with vigorous agitation every 10 min. After digestion, the suspension was centrifuged at 200 × g for 10 min, and the supernatant was transferred to a new tube. The remaining pellet was treated with prewarmed 0.25% trypsin–EDTA (Gibco) and incubated at 37 °C for 20 min.

The cell suspensions were centrifuged and resuspended in Ham's F-10 medium supplemented with 20% fetal bovine serum (FBS; Gibco), 1% Primocin (InvivoGen), and DMEM High Glucose medium supplemented with 4 mM GlutaMAX (Gibco) and 5 ng mL^{-1} basic fibroblast growth factor (bFGF; Thermo Scientific). Finally, the pooled cell suspension was filtered through a 40 μm cell strainer and seeded for culture.

2.4.2 Cell growth experiments

Different scaffold formulations were evaluated regarding their ability to support cell adhesion and proliferation. The scaffolds were transferred to ultra-low-attachment plates (Corning) at a final working volume of 10 mL per well. Prior to cell seeding, the scaffolds were carefully washed with sterile DPBS to remove residual materials.

Cells were seeded at a density of 1×10^6 cells per scaffold and maintained under static culture conditions at 37 °C in a humidified atmosphere containing 5% CO_2. On days 2 and 7 of culture, cells were recovered for analysis.

For cell dissociation, the scaffolds were removed from the culture plates, transferred to new plates, and incubated with TrypLE solution (Gibco) until complete cell detachment. After digestion, total cell number and cell viability were determined using the Trypan Blue exclusion assay with a Countess 3 Automated Cell Counter (Thermo Fisher Scientific), according to the manufacturer's instructions.

To confirm complete cell dissociation, the scaffolds were stained with DAPI (4′,6-diamidino-2-phenylindole) after cell collection to verify the absence of residual cells. Additionally, bovine myoblasts/myotubes were characterized by immunohistochemistry. Cells were fixed with 4% paraformaldehyde, permeabilized with 0.5% Triton X-100, and blocked with goat serum or BSA. Samples were incubated overnight at 4 °C with rabbit anti-ITGA7 primary antibody (Sunlong Biotech), followed by Alexa Fluor 488-conjugated secondary antibody incubation (Thermo Scientific). F-actin and nuclei were counterstained with Rhodamine

Phalloidin and Hoechst 33342, respectively. Fluorescently labeled cells were visualized using an EVOS M7000 fluorescence microscope (Thermo Scientific).

2.4.3 Cell differentiation experiments

Cell differentiation experiments were conducted under static culture conditions, with the scaffold formulations serving as support matrices for muscle cell growth. The scaffolds seeded with C2C12 cells (data not shown) and bovine satellite cells were maintained under culture conditions for up to 7 days to evaluate cell expansion and distribution throughout the porous structure.

2.4.4 Immunofluorescence assay

Cell viability within the scaffolds was evaluated using fluorescent staining with Ethidium Homodimer-1 (excitation/emission: ~528/617 nm) and Calcein AM (excitation/emission: ~494/517 nm) (Invitrogen–Thermo Fisher Scientific, USA) to visualize dead and viable cells, respectively.

For the Live/Dead assay, the fluorescent dyes were diluted to 2 μM in PBS from their stock solutions. The scaffolds were incubated in the staining solution for 1 h at room temperature in the dark and subsequently examined under a fluorescence microscope on days 2 and 7 of culture. All assays were performed in triplicate.

2.5 Statistics

All experiments were performed in triplicate. Results are presented as mean ± standard deviation. Statistical analysis was performed using one-way ANOVA followed by Tukey's post hoc test. Differences were considered significant at $p < 0.05$ (Statistica® 13.5, StatSoft Inc., USA).

3 RESULTS AND DISCUSSION

3.2 Morphology characterization

The developed scaffolds exhibited stable macroscopic structures and maintained adequate integrity after freeze-drying, regardless of the concentration of OKP incorporated into the formulations. Visual evaluation demonstrated that the matrices maintained their structural cohesion and handling properties, indicating that the addition of OKP did not compromise scaffold formation. The macroscopic morphology and visual appearance of the lyophilized scaffolds are presented in Figure 2.

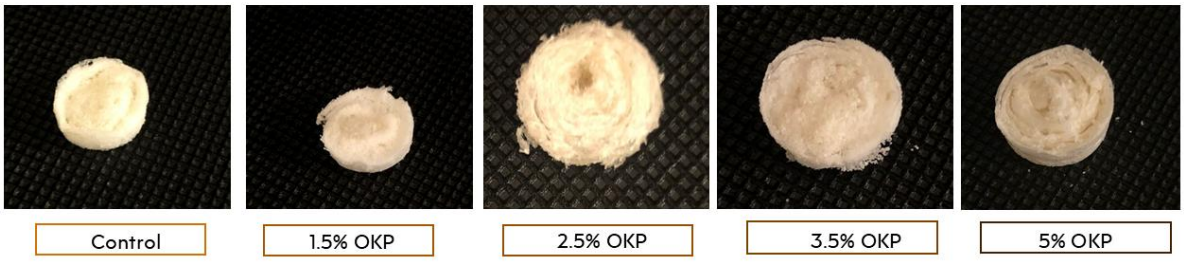


Fig. 2 Visual appearance and macroscopic morphology of lyophilized scaffolds containing different concentrations of okara powder (OKP).

The incorporation of OKP did not compromise the structural integrity of the matrices, preserving the cohesion required for handling and subsequent applications. Since the physical and mechanical properties of

scaffolds are critical for in vitro performance and directly influence cellular responses (Foley and Floreani, 2025), parameters such as porosity, swelling behavior, biodegradation, biocompatibility, and dimensional stability must be carefully evaluated to determine whether the scaffolds can provide adequate mechanical support and maintain structural integrity throughout the cell culture process (Shang et al., 2025). In this context, scaffold diameter and thickness are particularly important, as these parameters directly affect mass transfer, nutrient diffusion, and the available surface area for cell attachment and proliferation. The diameter and thickness values of the scaffolds formulated with different concentrations of OKP are presented in Table 1.

Table 1 Diameter and thickness of the scaffolds.

Sample	Diameter (mm)	Thickness (mm)
Control	$9.65^{b} \pm 0.49$	$2.40^{b} \pm 0.00$
1.5% OKP	$11.45^{a} \pm 0.35$	$3.00^{ab} \pm 0.14$
2.5% OKP	$11.90^{a} \pm 0.56$	$3.30^{a} \pm 0.14$
3.5% OKP	$12.25^{a} \pm 0.49$	$2.40^{b} \pm 0.14$
5% OKP	$12.50^{a} \pm 0.14$	$3.45^{a} \pm 0.07$

Values are expressed as means of triplicate ± standard deviation. Different letters in the same row indicate significant differences ($p < 0.05$). OKP: Okara powder.

The incorporation of okara significantly influenced the structural dimensions of the matrices ($p < 0.05$). The control scaffold exhibited the smallest diameter (9.65 mm), whereas scaffolds containing OKP showed significantly larger diameters ($p < 0.05$), ranging from 11.45 to 12.50 mm, corresponding to an increase of up to 30% in the 5% OKP formulation relative to the control. Although okara is generally characterized by a low water-holding capacity due to the predominance of insoluble dietary fibers (Cheng et al., 2026), the dimensional expansion observed in the present study suggests a distinct behavior when OKP is incorporated into soy protein isolate–sodium alginate matrices. This effect may be associated with changes in the organization of the polymeric network, leading to enhanced matrix expansion and greater water retention within the hydrogel.

This behavior can be attributed to the structuring effect of fibers and polysaccharides, which likely reduced polymer network shrinkage during lyophilization while promoting the formation of more porous architectures (Wang et al., 2026). From a tissue-engineering perspective applied to cultivated-meat production, such dimensional expansion is particularly advantageous, as it increases the available surface area for cell adhesion and migration and facilitates oxygen and nutrient diffusion throughout the scaffold (Korkeamäki et al., 2024).

Regarding thickness, the control scaffold measured 2.40 mm, whereas formulations containing OKP ranged from 2.40 to 3.45 mm. These values were higher than those reported by Chien and Shah (2012) for soy protein isolate-based scaffolds, which ranged from 1.7 to 2.4 mm. The highest thickness observed in the scaffold containing 5% OKP suggests that higher concentrations of okara may contribute to the formation of thicker matrices, possibly due to increased viscosity of the scaffold-forming suspension and the higher content of structural solids, which improve network stability during freeze-drying (Offeddu et al., 2016).

In general, thicker scaffolds tend to exhibit greater firmness and easier handling properties. Moreover, thicker matrices may exhibit a lower fiber diameter, improved load-bearing capacity, and reduced structural rigidity, characteristics that can favor both cell adhesion and material resistance during experimental manipulation (Kimura and Zanin, 2024). Scaffold thickness is therefore an important parameter in scaffold development, as it is closely associated with cell adhesion, spreading, and proliferation (Uygun et al., 2010). The results are consistent with trends reported in the literature and reinforce the importance of dimensional control in ensuring scaffold reproducibility and structural quality. Scaffold geometry and shape can be tailored to generate structures with specific dimensions, directly influencing tissue organization and the structural characteristics of the final product (Kawecki et al., 2024).

To further investigate the influence of okara incorporation on the structural organization of the matrices, SEM and porosity analyses were performed. Scaffold porosity is a key factor for reproducing the three-dimensional microenvironment found in vivo, directly influencing cell interactions, cell migration, and oxygen and nutrient transport throughout the matrix (Mukasheva et al., 2024). Parameters such as pore size, pore distribution, and pore interconnectivity play an important role in cell adhesion, proliferation, and organization in tissue engineering systems (Ding et al., 2026). Figure 3 presents SEM micrographs of the scaffolds obtained at magnifications of 50×, 150×, and 1000×.

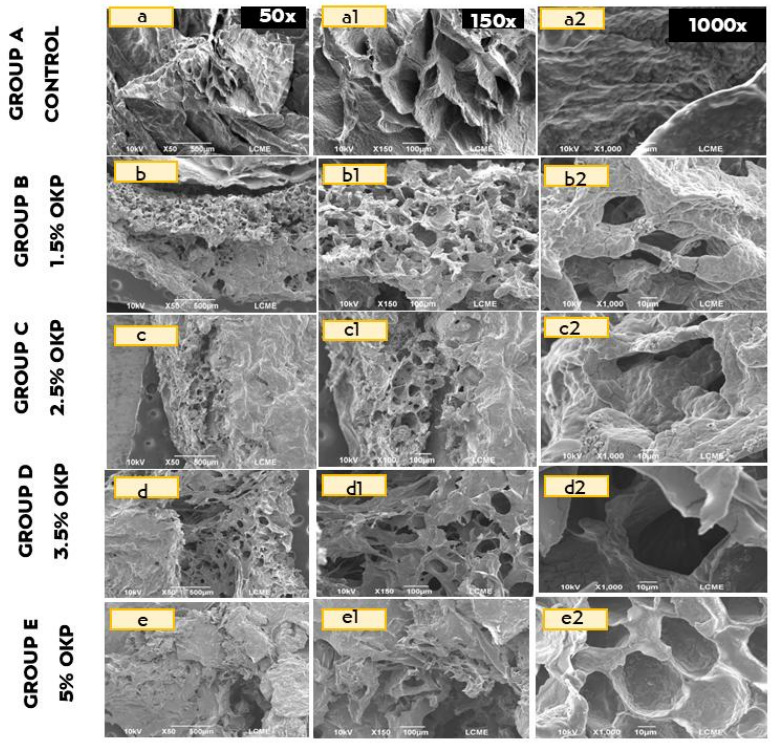


Fig. 3 Scanning electron microscopy (SEM) micrographs of sodium alginate-based scaffolds functionalized with okara protein and yerba mate polyphenols. Rows represent the experimental groups: (a) alginate control; (b) 1.5% OKP; (c) 2.5% OKP; (d) 3.5% OKP; and (e) 5.0% OKP (w/v). Columns indicate magnifications of 50×, 150×, and 1000×. White scale bars in the 1000× micrographs represent 10 µm. OKP: Okara powder.

The SEM micrographs revealed important differences in scaffold microstructure and porosity as a function of OKP incorporation. Since all scaffolds underwent the same freeze-drying process, the observed

morphological differences are primarily attributable to variations in matrix composition. Overall, the incorporation of okara promoted structural modifications resulting in a more porous and interconnected three-dimensional network, a characteristic considered highly desirable for cultured meat applications (Wensing et al., 2025).

The control scaffold exhibited a relatively compact and less porous surface, characterized by a lamellar structure with few visible pores. This morphology indicates the formation of a denser matrix, which may compromise the formation of interconnected pores and, consequently, reduce the diffusion of essential molecules, such as oxygen and nutrients, throughout the scaffold. Therefore, porosity optimization becomes essential to support initial cell survival and enable cultured meat production (Hudson et al., 2025).

After OKP incorporation into the formulations, a marked change in matrix organization was observed. The images revealed the formation of larger, better-defined pores and a more open three-dimensional structure. This behavior may be attributed to the presence of fibers and structural components from okara, which likely contributed to the formation of a more heterogeneous network during scaffold formation (Xu et al., 2026).

In the intermediate formulations (1.5 and 2.5% OKP), interconnected pores were already observed, which may favor cell migration and nutrient diffusion. Pore interconnectivity is considered one of the most important parameters in tissue-engineering scaffold design because it allows cells to distribute throughout the matrix and enables efficient culture medium circulation (Picado-Tejero et al., 2025). In scaffolds with higher OKP concentrations (3.5% and 5%), the microstructure exhibited larger, more well-defined pores, forming a more pronounced three-dimensional network. This porous architecture is fundamental for facilitating rapid water absorption, swelling behavior, and diffusion of solutes and biomolecules through the hydrogel matrix (Ganguly et al., 2025).

Another relevant aspect observed in the micrographs was the irregular morphology of the pore walls, a common characteristic of plant-derived biomaterials. This irregularity may favor cell anchorage by increasing surface roughness and enlarging the contact area between cells and the scaffold. In tissue engineering applications, rough surfaces may provide more cell-adhesion sites (Golubchikov et al., 2026). In addition, scaffolds produced from plant-derived raw materials, such as okara, may exhibit a well-organized architecture optimized for fluid transport and cell–matrix interactions (Vargas-Ovalle et al., 2025).

To complement the qualitative evaluation of the SEM images, porosity and pore diameter distribution were quantified using the 1000× micrographs. Through thresholding of the SEM images, the void areas of the matrices were isolated and converted into quantitative porosity data. The porosity values are presented in Table 2.

Table 2. Porosity of the scaffolds calculated using ImageJ software.

Group	Porosity
Control	43.07%
1.5% OKP	15.48%
2.5% OKP	31.51%
3.5% OKP	40.70%
5% OKP	63.00%

OKP: Okara powder.

The control scaffold exhibited 43% porosity, indicating a relatively organized matrix with a lower volume of void space available for diffusion. The addition of 1.5% OKP resulted in a marked reduction in porosity (15%), possibly associated with increased matrix density and partial pore obstruction caused by the solid fraction of okara. This behavior suggests that low OKP concentrations may impair the formation of an interconnected porous network.

With increasing OKP concentration to 2.5% and 3.5%, a gradual recovery in porosity was observed (31.51% and 40.70%, respectively), indicating structural reorganization of the system. This effect may be related to the balance between suspension viscosity and the ability to form more open structures during freezing and lyophilization. Notably, the scaffold containing 5% OKP exhibited the highest porosity (63%), suggesting that higher okara concentrations favor the formation of a more expanded three-dimensional network with a greater void volume. These results are consistent with reports in the literature recommending porosity values between 30 and 90% for tissue-engineering scaffolds (Moslemy et al., 2023). The complementary analysis of the pore diameter distribution histograms presented in Figure 4 enabled a more detailed evaluation of the scaffolds' internal architecture.

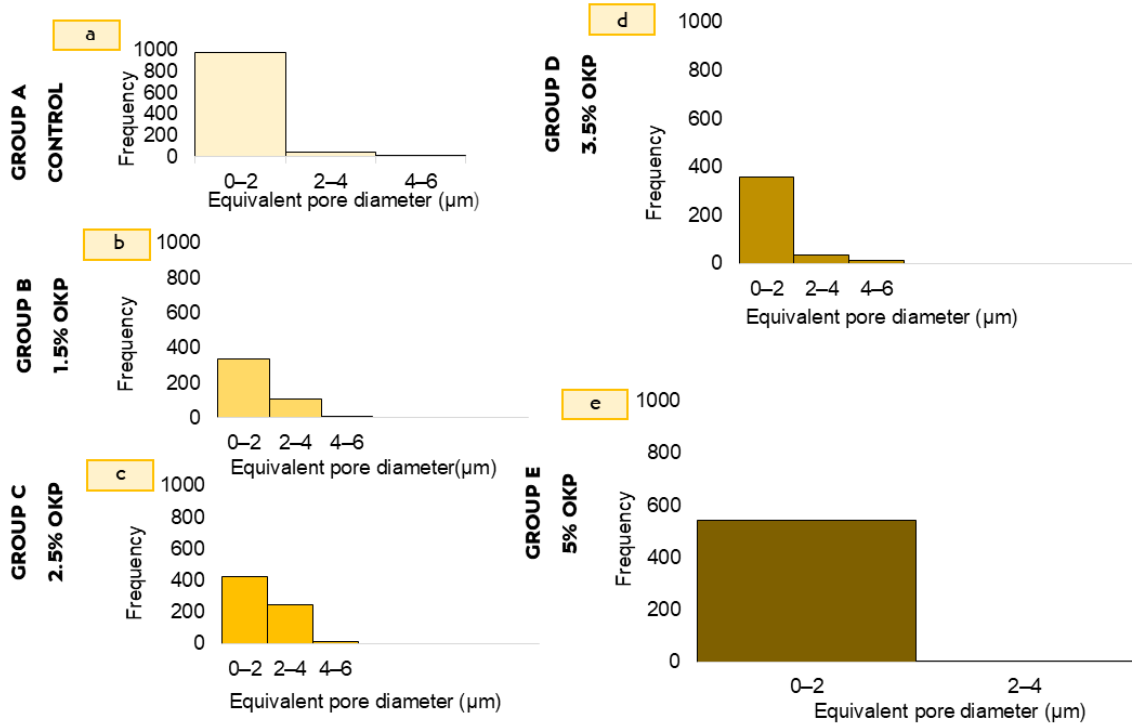


Fig. 4 Frequency distribution of equivalent pore diameter in the scaffolds for groups (a) Control; (b) 1.5% OKP; (c) 2.5% OKP; (d) 3.5% OKP; and (e) 5.0% OKP. OKP: Okara powder.

The pore diameter distribution histograms presented in Figure 4 provided additional information on the scaffold's internal architecture. A predominance of pores in the 1.0 – 2.0 µm range was observed, suggesting potential suitability for cell culture applications. Previous studies, such as that reported by Okada et al. (2026), employed culture inserts with pores of approximately 1.0 µm (Corning®) to establish controlled microenvironments. In this context, the dimensional similarity observed in the present study suggests that the developed scaffolds may facilitate nutrient and metabolite diffusion, thereby helping maintain cell viability in

three-dimensional systems. Overall, the SEM and ImageJ porosity analyses demonstrated that incorporating okara promoted the formation of more porous, three-dimensional structures, characteristics considered highly desirable for scaffold applications in cultured meat production.

3.3 Mechanical properties

In biological environments, cells are frequently exposed to tangential forces known as shear stress, generated by the flow of water or physiological fluids around cell surfaces. Consequently, cells must respond appropriately to these physical forces to grow, adapt, and survive within complex microenvironments (Mishra; Peter, 2022). The cellular response to shear stress is directly related to the system's bioactivity, as processes such as cell adhesion, proliferation, and differentiation depend on both the diffusion of oxygen and nutrients through the porous structure and the mechanical forces induced by fluid flow within the scaffolds. In this context, fluid-induced shear stress is frequently described as one of the primary mechanical stimuli that can modulate the proliferation and differentiation of scaffolds (Ali et al., 2020).

In the context of cultivated meat production, scaffolds play a fundamental role in modulating shear stress, as their porous structure can influence fluid flow distribution and, consequently, the magnitude of shear stress to which cells are exposed. Inadequately designed structures can trigger cellular damage or compromise the biomaterial's performance. Thus, determining shear stress in scaffolds becomes a crucial parameter for their application in cultivated meat production. Table 3 presents the shear stress and compression results for the scaffolds produced with different concentrations of OKP.

Table 3 Mechanical properties of sodium alginate scaffolds as a function of okara powder (OKP) concentration.

Group	Shear stress (N)	Maximum Compression Force (N)
Control	15.94±1.05[a]	0.09±0.004[a]
1.5% OKP	13.32±1.32[a]	0.097±0.002[a]
2.5% OKP	14.00±0.85[a]	0.092±0.004[a]
3.5% OKP	15.18±0.82[a]	0.096±0.006[a]
5% OKP	12.73±1.28[a]	0.136±0.027[a]

Values represent the mean ± standard deviation (n = 3). Different superscript letters in the same column indicate statistically significant differences according to Tukey's test ($p < 0.05$). OKP: Okara powder.

High maximum compression forces can compromise cell adhesion and behavior, as excessively rigid substrates tend to hinder processes such as proliferation and differentiation (Discher et al., 2005). In the present study, the scaffold containing 5.0% OKP showed the highest mean maximum compression force (0.136 N) compared with the other formulations. However, no statistically significant differences were observed between the groups ($p > 0.05$), indicating that the incorporation of OKP did not lead to meaningful changes in the global mechanical strength of the scaffolds.

Generally, materials with higher porosity tend to exhibit lower compressive resistance due to structural voids that act as stress concentrators and promote failure mechanisms (Gharivi et al., 2025). Regarding the results obtained in this study, shear stress values ranged from 12.73 to 15.94 N, with the highest mean recorded for the control scaffold (15.94 N) and the lowest for the formulation containing 5.0% OKP (12.73 N).

Although a downward trend in stress is observed with increasing OKP concentration, statistical analysis indicated no significant difference between the formulations ($p > 0.05$), as indicated by the same letters in the graph.

Despite the lack of a statistically significant difference, the observed gradual reduction may be attributable to structural modifications induced by the incorporation of okara into the polymeric matrix. As previously discussed, increasing the okara content promoted changes in dimensions and, possibly, in the porosity of the matrices, factors that directly influence fluid flow behavior within the structure (Zhao, Vaughan, and McNamara, 2016). More porous structures with higher interconnectivity tend to promote a more homogeneous flow distribution, reducing local shear stress concentrations and fostering a more favorable mechanical microenvironment for cell growth. The porous architecture of the scaffolds plays a fundamental role in modulating internal shear stress, as pore geometry and size directly influence matrix permeability and fluid flow distribution (Singh et al., 2023).

In this sense, permeability and wall shear stress stand out as relevant parameters, as they are directly related to cellular activity in the scaffolds: while permeability facilitates the transport of nutrients and metabolites, shear stress acts as a mechanical stimulus perceived by cells, contributing to differentiation and proliferation. In cultivated meat production, these aspects are particularly relevant, as moderate shear stress can stimulate cellular processes without compromising structural integrity. Conversely, excessive shear stress can induce cell detachment from scaffolds, impairing adhesion and limiting cellular expansion (Sun et al., 2025).

The absence of a statistically significant difference between the control scaffold and the OKP formulations should be interpreted in light of the microstructural analyses. Scanning electron microscopy (SEM) images evidenced that the control scaffold presents a more compact and denser matrix (Figure 3a), whereas the 5.0% OKP formulation exhibits a highly porous and interconnected structure (Figure 3e), with a porosity of approximately 43.07% (Tu et al., 2023; Bodiou et al., 2023). In conventional polymeric systems, an increase in porosity of this magnitude would typically result in a significant reduction in mechanical strength. However, the observed stiffness suggests that okara structural components, especially fibers and insoluble proteins, act as microstructural reinforcing agents. This compensatory effect indicates that even with a reduction in the matrix's continuous solid fraction, a structural network capable of sustaining mechanical loads is formed, possibly due to interactions between biopolymers and the contribution of fibrous particles as reinforcement elements. This behavior demonstrates a synergy between composition and architecture, reconciling high porosity with mechanical stability.

3.4 Swelling ratio and biodegradation

The ability of scaffolds to absorb water and swell was measured to evaluate the effectiveness of nutrient mass transfer after potential cell seeding. Theoretically, scaffolds exhibiting a high initial swelling rate provide a favorable environment and volumetric space for cell proliferation. Figure 5 presents the swelling ratio variation of the scaffolds as a function of time (4, 24, 48, and 72 h) and different OKP concentrations.

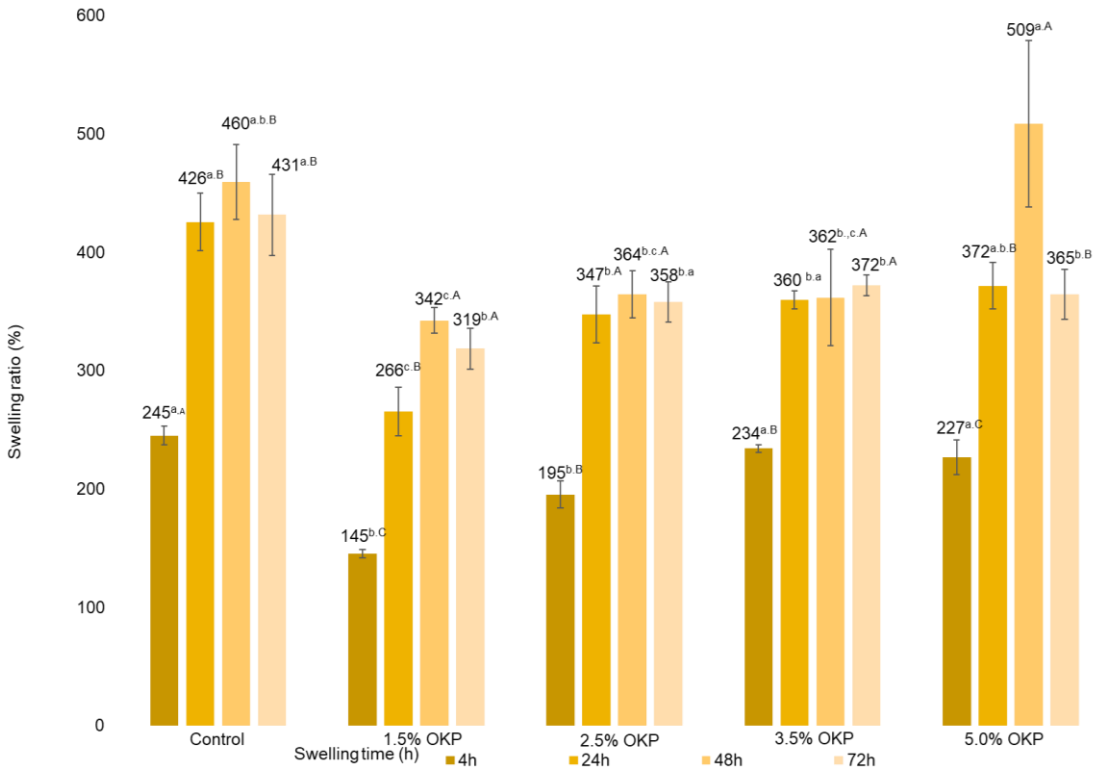


Fig. 5 Swelling ratio (%) of sodium alginate scaffolds as a function of immersion time and okara powder (OKP) concentration. Data are expressed as mean ± standard deviation (n = 3). Different lowercase letters indicate significant differences between the control and OKP concentrations within the same time point. Different uppercase letters indicate significant differences over immersion time for the same formulation ($p < 0.05$).

The incorporation of pores into hydrogels can facilitate cell proliferation by creating void spaces and favoring the exchange of nutrients and metabolites between the material's interior and the surrounding medium (Yu, Wu, & Zhang, 2026). In this context, the formulation containing 5.0% OKP exhibited the highest expansion and water-retention capacity. This behavior is consistent with the porosity data obtained via ImageJ, in which this sample was identified as the most porous (63%), suggesting that a larger fraction of small-diameter pores may favor fluid entry through capillarity. The addition of okara proteins and fibers may interact with the alginate matrix, possibly through hydrogen bonding between polar groups, such as the carboxyl groups of alginate and the amine/amide groups of proteins, which can modulate the hydrophilic properties of the system (Krunic & Osmokrovic, 2026).

Regarding swelling kinetics, during the first 4 h, all scaffolds showed the lowest absorption values, characterizing the initial stage of hydration and surface diffusion. Between 4 and 24 h, a sharp and statistically significant increase in fluid retention was observed. For most groups, values reached a statistical plateau between 48 and 72 h, indicating an approach toward swelling equilibrium. At this stage, the osmotic pressure of water entry is counterbalanced by the elastic retraction forces of the polymer network's cross-links (Nakajima et al., 2021). The stabilization observed at 72 h indicates good structural stability, suggesting that the scaffold maintains its integrity even under high hydration levels. Conversely, formulations with lower OKP contents (1.5% and 2.5%) exhibited lower swelling rates than the control at various intervals. This may be associated with

a more compact structural organization, in which interactions between the solid fraction of okara and the polymer reduce the free volume available for matrix expansion.

Complementary to the swelling behavior, the in vitro degradation of the formulated scaffolds (Figure 6) was calculated by the mass loss of dry samples in PBS (37 °C; pH 7.4) over 3 days.

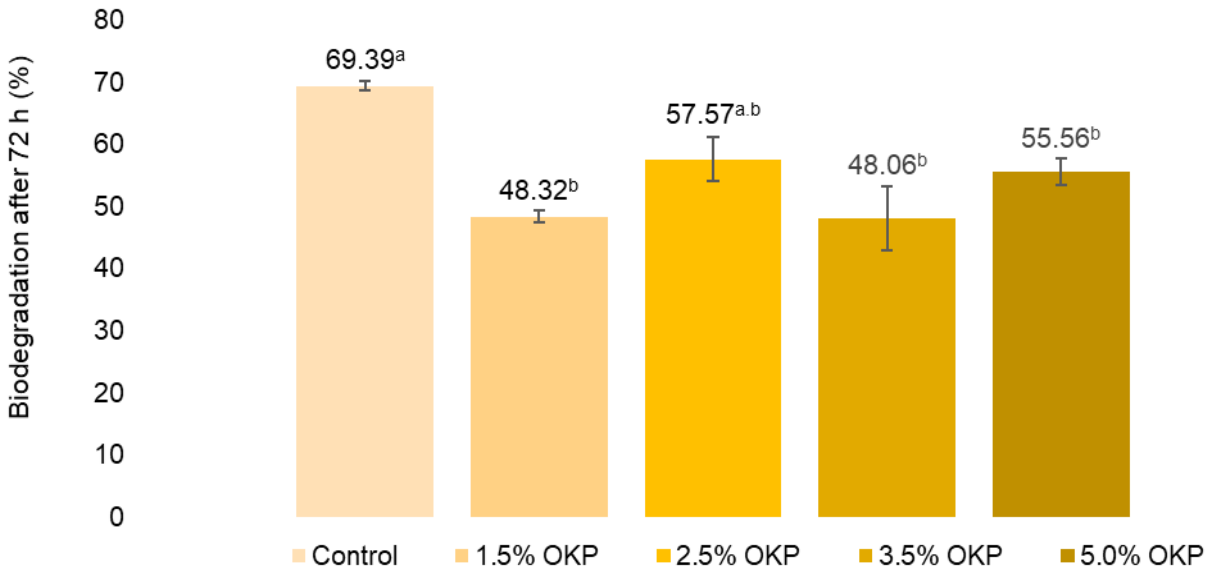


Fig. 6 In vitro biodegradation (mass loss %) of lyophilized scaffolds after 72 h of immersion in phosphate-buffered saline (PBS) medium (pH 7.4; 37 °C). Data are expressed as mean ± standard deviation (n = 3). Different lowercase letters indicate significant differences between formulations, as determined by Tukey's test ($p < 0.05$). OKP: Okara powder.

Control scaffolds degraded more rapidly than those with added OKP, losing approximately 70% of their mass within 3 days. In contrast, scaffolds with 1.5%, 2.5%, 3.5%, and 5.0% OKP concentrations lost between 48% and 58% of their initial mass after 3 days, showing significantly lower mass loss than the control ($p < 0.05$). Scaffold degradability was evaluated to assess structural compatibility and temporal stability of the support prior to full cellular maturation. The primary reason for the higher degradation rate observed in the control group is the instability of the gel network formed exclusively by sodium alginate when exposed to ion exchange and hydrolysis in an aqueous medium, thereby accelerating matrix disintegration (Zhao, 2000). On the other hand, the combination of proteins and polysaccharides from okara acts as a network stabilizing agent (Yan et al., 2022). The interaction between okara proteins and alginate creates a more robust structure, possibly through hydrogen bonds and electrostatic interactions, providing greater resistance to mechanical and chemical erosion of the scaffold (Qi & Wen, et al., 2026). Although a low degradation rate is essential for maintaining the support morphology and providing mechanical stability to cells (Piasecki et al., 2003), an appropriate level of degradation is desirable and strategic in tissue engineering. Since the scaffold is composed primarily of biopolymers, the substances produced during its degradation, such as readily assimilable peptides and polysaccharides, can serve as supplementary nutrients for cell growth, thereby promoting proliferation and the formation of new tissues (Smoak et al., 2021). Therefore, the degradation rate observed for the 5.0% OKP scaffolds (55%) highlights a balance between the structural persistence required for initial cell adhesion and the gradual release of bioactive components. This controlled degradation profile is conducive to continuous cell

differentiation and myotube formation, which are fundamental characteristics for the viability of these supports in cultivated meat production (Fan et al., 2019).

3.5 Chemical characterization

The ATR-FTIR spectra of the control and OKP-functionalized scaffolds (1.5%, 2.5%, 3.5%, and 5.0% OKP) are shown in Figure 7.

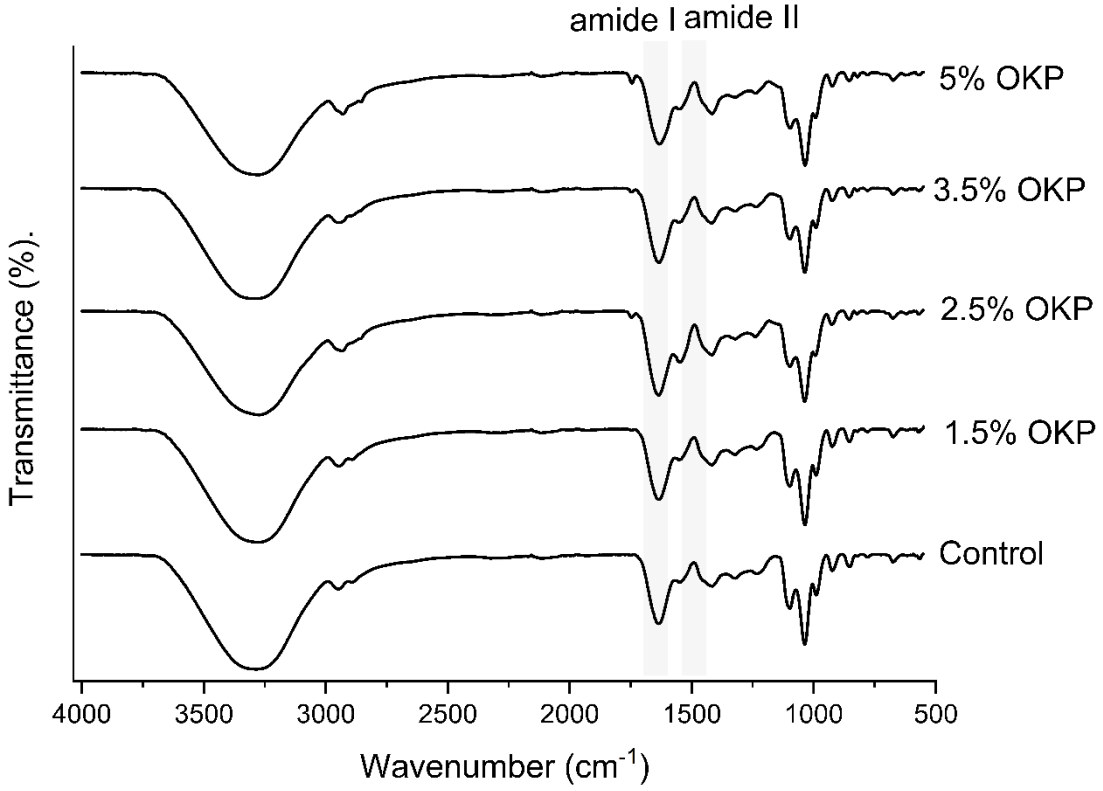


Fig. 7 Attenuated Total Reflectance Fourier Transform Infrared Spectroscopy (ATR-FTIR) spectra of sodium alginate scaffolds functionalized with different concentrations of okara powder (OKP) and yerba mate extract. The shaded areas highlight the Amide I and Amide II bands.

Spectral analysis confirmed the presence of the primary functional groups associated with the scaffold constituents. The band observed between 1040–1050 cm^{-1} is attributed to polyphenols in the yerba mate extract (Alibadi et al., 2020), suggesting their successful retention within the matrix. Furthermore, the bands observed in the 3000–3650 cm^{-1} region are consistent with those reported for okara, attributed to O–H stretching vibrations associated with cellulose and hemicellulose, which are the main constituents of the okara fibrous fraction (Adeyanju & Adebo, 2025).

Despite varying OKP concentrations, the scaffolds' spectral profiles showed no significant shifts or notable changes in band intensity. These results indicate that the OKP concentration did not promote detectable chemical alterations in the matrix. This behavior highlights the molecular compatibility between the formulation components, okara, soy protein isolate, alginate, and yerba mate extract. It can be attributed to the formation of a stabilized network, primarily via intermolecular interactions such as hydrogen bonding (associated with the 3000–3600 cm^{-1} region), along with other non-covalent physical interactions.

The bands corresponding to Amide I (~1650 cm^{-1}) and Amide II (~1550 cm^{-1}), highlighted in the spectra, are related to C=O stretching and N–H bending vibrations, respectively, which are characteristic of peptide bonds. The maintenance of these bands without significant changes indicates preservation of the protein's secondary structure, demonstrating that incorporating the different components did not compromise the protein conformation within the scaffolds.

ATR-FTIR analysis confirmed the chemical stability of the matrix, demonstrating that OKP incorporation did not alter the primary functional groups but rather promoted a network stabilized by robust intermolecular interactions. This chemical stability is directly reflected in the biodegradation assays, where the presence of OKP acted as a structural reinforcing element, reducing mass loss. This delayed degradation is fundamental to ensuring the mechanical integrity required during the critical initial stages of cell adhesion and proliferation.

3.6 *In vitro* digestibility

Achieving an optimal balance among mechanical performance, digestibility, and structural fidelity remains a major challenge in the development of scaffolds for cultivated meat applications (Zo et al., 2025). To evaluate their degradation behavior under physiological conditions, scaffolds containing different concentrations OKP were subjected to simulated oral, gastric, and intestinal digestion. Figure 8 illustrates the release profiles of polysaccharides (a), total phenolic compounds (b), and antioxidant activity (c) throughout the in vitro gastrointestinal digestion process.

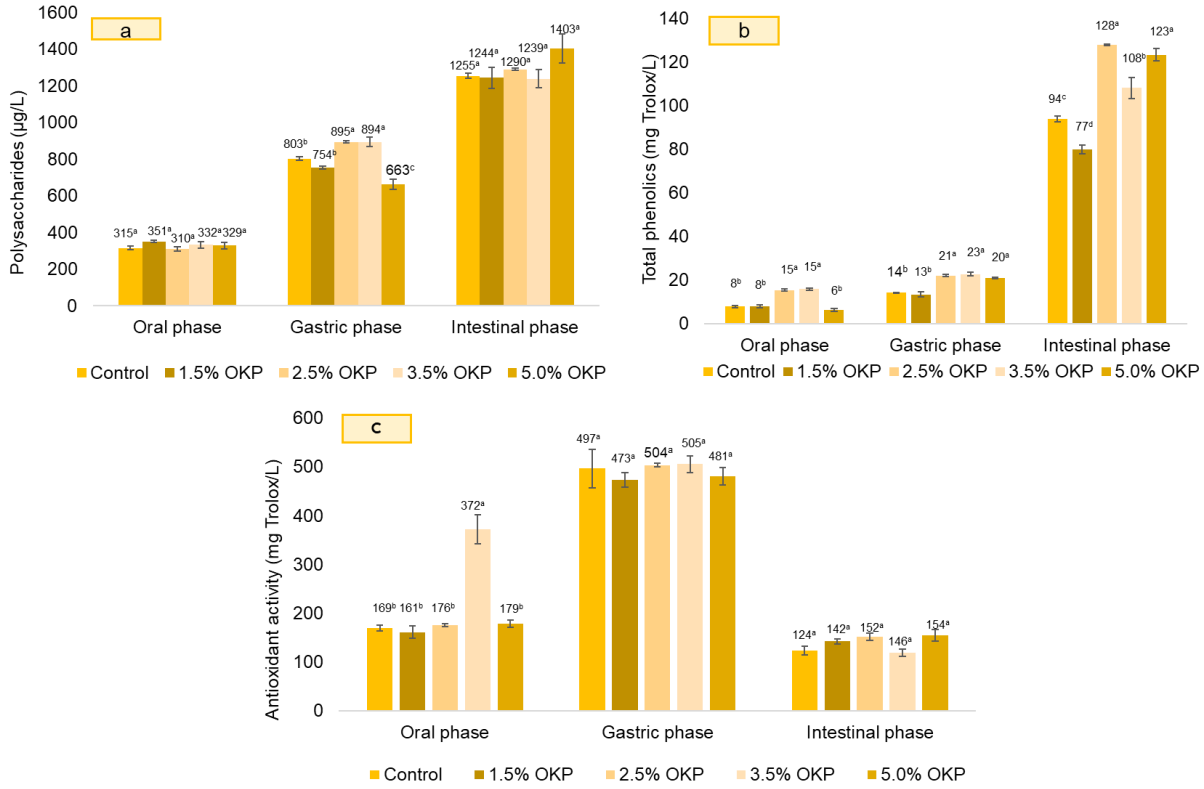


Fig. 8 *In vitro* gastrointestinal digestion profile of alginate-okara scaffolds. (A) Polysaccharide release (µg/L); (B) Total phenolic content (mg Trolox/L); and (C) Antioxidant activity (mg Trolox/L) throughout the oral,

gastric, and intestinal phases. Data are expressed as mean ± standard deviation (n = 3). Different letters within the same digestive phase indicate significant differences between formulations, as determined by Tukey's test ($p < 0.05$). OKP: Okara powder.

In the initial oral phase, the concentration of released polysaccharides ranged between 310 ± 10 µg/L and 351 ± 5 µg/L. At this stage, no statistically significant differences ($p > 0.05$) were observed among the concentrations, indicating preliminary stability of the alginate-okara matrix at salivary pH. Upon transitioning to the gastric phase, an increase in polysaccharide release was observed (from 663.27 to 894.90 µg/L), indicating the onset of matrix degradation. However, statistically significant differences were observed between the control and the samples with intermediate OKP concentrations (2.5% and 3.5%), which showed higher release rates. In contrast, the 5.0% OKP sample exhibited the lowest release rate (663.27 ± 27.42 µg/L) ($p < 0.05$). This behavior suggests that a denser network, characterized by stronger protein-polysaccharide interactions, hinders enzymatic diffusion and delays matrix erosion in acidic media.

The highest scaffold degradation was observed during the intestinal phase, with polysaccharide release values ranging from 1239 ± 50 µg/L to 1403 ± 79 µg/L. At this stage, the combined action of pancreatic enzymes and the transition to mildly alkaline pH promotes alginate depolymerization and the solubilization of okara-derived fibers, resulting in extensive matrix disintegration (Madsen et al., 2022). The absence of significant differences among formulations at the end of the intestinal phase indicates that scaffold digestibility was not compromised by incorporating different OKP concentrations. This progressive degradation behavior is particularly relevant for controlled-release applications, as protein–polysaccharide interactions can modulate the retention and release kinetics of bioactive compounds (Sabaghi et al., 2022).

In the developed scaffolds, the interaction between OKP and sodium alginate likely formed a complex polymeric network that entrapped yerba mate phenolic compounds and promoted their sustained release during hydrolytic degradation of the matrix. Such a progressive release profile is highly desirable, as it preserves antioxidant activity and enhances the bioaccessibility of these compounds throughout gastrointestinal digestion.

Total phenolic release (Figure 8b) varied throughout the *in vitro* digestion, with values ranging from 6.43 ± 0.67 to 15.83 ± 0.51 mg Trolox/L in the oral phase, 13.45 ± 1.18 to 22.74 ± 0.84 mg Trolox/L in the gastric phase, and 79.76 ± 2.02 to 127.86 ± 0.34 mg Trolox/L in the intestinal phase, consistent with the previously observed increase in polysaccharide release. This suggests that the progressive degradation of the protein-alginate matrix under intestinal conditions favored the release of phenolic compounds from the incorporated yerba mate extract. However, no clear trend in phenolic release with OKP content was observed, suggesting that the digestive conditions themselves predominantly influenced the release profile.

Antioxidant activity also varied throughout *in vitro* digestion (Figure 8c). Phenolic compounds from the yerba mate extract maintained their free radical scavenging capacity after incorporation into the scaffold matrix and exposure to simulated digestive conditions. The highest antioxidant activity values were found in the gastric phase (473.15 ± 15.03 to 505.63 ± 16.79 mg Trolox/L), suggesting greater accessibility of these compounds in acidic media, possibly due to their solubilization and matrix swelling, which favored their exposure and interaction with the DPPH radical. No significant differences ($p > 0.05$) in antioxidant activity were observed across the different OKP concentrations.

From a biochemical perspective, the changes observed during *in vitro* digestion can be attributed to the combined action of pH and digestive enzymes on the protein-alginate matrix. In gastric medium, an acidic pH promotes protein denaturation and swelling of the polymeric network, favoring structural reorganization and exposing functional groups. Madsen et al. (2022) experimentally demonstrated that the interaction between alginate and proteins influences digestibility and structural dynamics, modulating enzymatic accessibility. Additionally, protein digestion in acidic media can yield peptides with potential antioxidant activity, while pH also influences the protonation state of phenolic compounds, thereby altering their reactivity (Shi et al., 2022).

During the intestinal phase, the combined action of pancreatin and bile salts further intensifies matrix deconstruction. It disrupts non-covalent interactions, including hydrogen bonding and electrostatic interactions, thereby promoting the release of previously retained phenolic compounds (Chen et al., 2025). These findings demonstrate that antioxidant activity is influenced not only by the concentration of released phenolics but also by structural and chemical modifications that occur during digestion. This behavior highlights the scaffold matrix as an active modulator of bioaccessibility and functionality, capable of controlling the release and preservation of bioactive compounds during gastrointestinal transit.

3.7 Cell culture

The selection of an appropriate cellular model is a critical determinant in cultivated meat research, as it dictates the technical and regulatory feasibility of the production process (Ravikumar et al., 2024). This choice is guided by proliferative capacity and differentiation potential, which directly impact process yield and the final product's nutritional profile (Robertson et al., 2024; Lim et al., 2024). In the present study, murine C2C12 myoblasts were used as a screening model to evaluate scaffold biocompatibility and cell adhesion. Subsequently, primary bovine myoblasts were used to validate scaffold performance with the target cell type for bovine muscle tissue engineering, thereby overcoming the limitations of relying exclusively on an immortalized cell line (Dai et al., 2024).

Phenotypic analysis was performed by immunocytochemistry using antibodies against integrin alpha 7 (ITGA7), as shown in Figure 9. Strong ITGA7 immunoreactivity was observed along the cell membrane and within the cytoplasm, confirming the myogenic origin of the bovine myoblasts. In addition, phalloidin staining revealed well-organized actin filaments and an elongated cellular morphology characteristic of adherent muscle cells. The merged fluorescence images demonstrated homogeneous distribution of ITGA7-positive cells with preserved cytoskeletal organization, indicating good cell integrity and maintenance of the myogenic phenotype throughout the culture period.

The resulting myotubes stained positively for both ITGA7 and phalloidin, demonstrating that bovine myoblasts successfully differentiated into linear, multinucleated myotubes within the functionalized scaffolds. The positive expression of ITGA7 further highlighted the bioactivity of the scaffolds, suggesting that the incorporation of okara proteins (OKP) and yerba mate polyphenols provided biological cues that promoted myoblast recognition and cell–matrix interactions. While phalloidin staining revealed cytoskeletal organization, ITGA7 expression confirmed effective cell–matrix communication, indicating that the scaffold microenvironment supported myogenic maturation and the formation of organized, multinucleated myotubes.

Based on the results of physical, mechanical, and chemical characterization (ATR-FTIR), the formulations containing 2.5% and 5% OKP were selected for the biological assays, as they exhibited a more

favorable balance between interconnected porosity, structural stability, and preservation of amide bands - features that are essential for cell recognition and adhesion. The control group served as a baseline reference for comparing the behavior of murine C2C12 myoblasts and primary bovine myoblasts, the latter representing the target cell type of the present study.

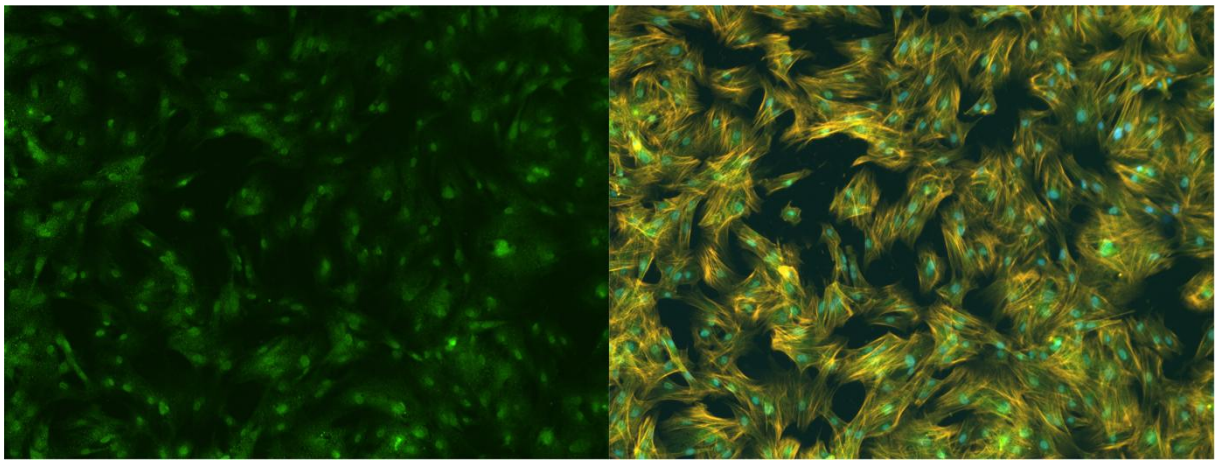


Fig. 9 Immunofluorescence analysis confirmed the myogenic phenotype of the bovine cells through positive staining for integrin alpha-7 (ITGA7, green) and F-actin (red).

3.7.1 Cell growth experiments

Quantitative proliferation assays were performed under static conditions with an initial seeding density of 10^6 myoblast cells per scaffold. Cell recovery via TrypLE digestion, followed by quantification with the Trypan Blue exclusion assay, demonstrated that all formulations supported cell viability and expansion over the 7 days (Table 4).

At 48 h, 5% OKP scaffolds exhibited the highest levels of cell adhesion and early proliferation, reaching a mean cell density of 2.82×10^5 cells. This value was markedly higher than those observed for Control and 2.5% OKP, which reached 1.48×10^5 and 1.05×10^5 cells, respectively. After 7 days of cultivation, 5% OKP exhibited pronounced exponential cell expansion, reaching an average of 2.56×10^6 cells, representing more than an eightfold increase relative to the 48 h time point.

In contrast, Groups Control and 2.5% OKP reached only 9.95×10^5 and 9.10×10^5 cells, respectively, over the same cultivation period (7 d). The enhanced performance of the 5% OKP formulation can be attributed to its elevated porosity (63%) and interconnected micropores (0–2 μm), which facilitate capillary-mediated nutrient transport and efficient metabolite exchange throughout the scaffold matrix. In addition, the preservation of the Amide I and II bands, as confirmed by ATR-FTIR analysis, indicates the maintenance of functional groups essential for cell adhesion and anchorage, thereby supporting effective cellular interactions without the need for additional cross-linking agents.

Table 4 Quantitative expansion of bovine myoblasts on OKP-functionalized scaffolds.

Group	48 h (cells/sample) x10^5	7 d (cells/sample) x10^5
Control	$1.48^{aA} \pm 0.65$	$9.95^{bA} \pm 1.98$
2.5% OKP	$1.05^{aA} \pm 0.15$	$9.10^{bA} \pm 3.09$
5.0% OKP	$2.82^{aB} \pm 0.33$	$25.7^{bB} \pm 5.86$

Proliferation of bovine myoblasts (1.10^6seeding density) on alginate-OKP scaffolds. Cell counts were performed in triplicate (n=3) after DAPI staining and trypsinization. Values are expressed as mean ± standard deviation. $^{a, A}$Different lowercase letters in the same row and uppercase letters in the same column indicate significant differences according to Tukey's test ($p < 0.05$); OKP: Okara powder.

The capacity of the developed scaffolds to support the transition from proliferating myoblasts to organized muscle-like structures was evaluated under static culture conditions. Quantitative analysis (Table 4) demonstrated that the 5% OKP formulation provided the most favorable microenvironment for cellular expansion, with a significantly higher cell density ($p < 0.05$) after 7 days of cultivation than in the other experimental groups.

This enhanced proliferative response was further corroborated by DAPI staining (Fig. 10), which revealed a homogeneous distribution of nuclei throughout the porous architecture, particularly within the 5% OKP scaffold after 7 days of culture. Moreover, the effectiveness of the cell recovery protocol was confirmed by the absence of residual nuclei following TrypLE treatment, as verified by post-dissociation DAPI staining. These findings demonstrate not only the efficient detachment of cells for quantitative analysis, but also the high capacity of the scaffolds to support deep cellular infiltration into their internal porous network.

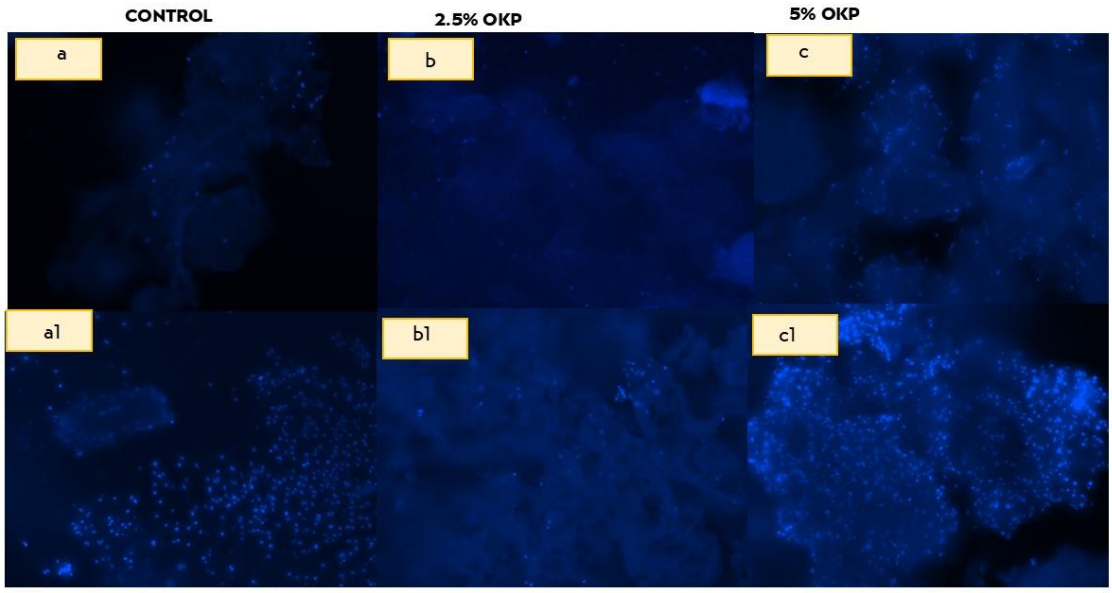


Fig. 10 Epi-fluorescence microscopy (DAPI) of bovine myoblasts attached to alginate-OKP scaffolds. a – c (48 h): Control, 2.5% OKP, and 5% OKP, respectively. a1 – c1 (7 days): Control, 2.5% OKP, and 5% OKP, respectively. Blue color indicates cell nuclei. Scale bar: 100 µm. OKP: Okara powder.

3.7.2 Cell differentiation experiments

The ability of the developed scaffolds to support the transition from proliferating myoblasts to organized muscle-like structures was evaluated under static conditions. The DAPI staining (Fig. 11) confirmed a homogeneous distribution of nuclei throughout the scaffolds' porous structure. Both C2C12 and bovine myoblasts demonstrated successful attachment and time-dependent proliferation, with the 5% OKP matrix showing the highest confluence after 7 days of culture.

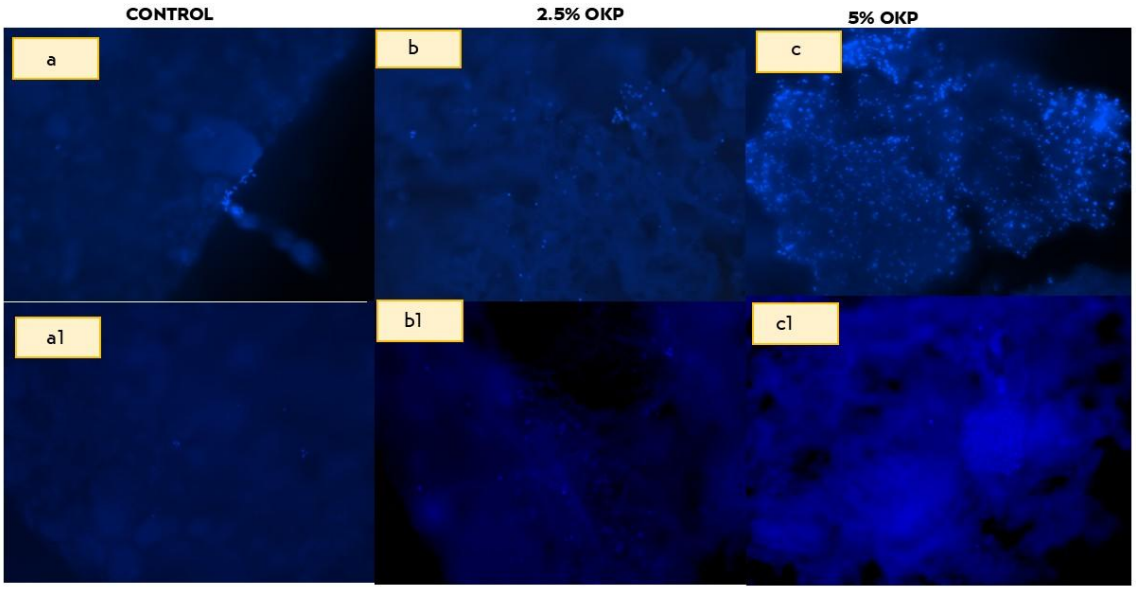


Fig. 11. Epi-fluorescence microscopy (DAPI) of cell adhesion and infiltration on selected scaffolds (Control, 2.5%, and 5.0% OKP). a – c: C2C12 lineage; a1 – c1: Bovine myoblasts. Blue color indicates cell nuclei. Scale bar: 100 µm. OKP: Okara powder.

The DAPI analysis results (Fig. 10) revealed a broad, homogeneous distribution of cell nuclei throughout the 5% OKP scaffold, indicating that the microporous network effectively promoted cellular infiltration. This formulation exhibited superior performance in increasing cell density for both the C2C12 lineage and primary bovine myoblasts compared to the control matrix. Complementarily, initial tests with bovine myoblasts confirmed the cellular adhesion capacity of the developed scaffolds even under initial culture conditions with a lower seeding density (1.10^4 cells). Taken together, these results demonstrate that scaffold architecture favors both cell infiltration and adhesion.

This biological performance is intrinsically linked to the developed porous architecture; the high porosity (63%) and pore refinement (0 – 2 µm) act synergistically to enhance capillary phenomena, ensuring high water retention, which corroborates the swelling results. This high hydrophilicity establishes an efficient microenvironment for the continuous diffusion of nutrients and the removal of metabolites, thereby sustaining cell viability even within the matrix's internal layers.

4 CONCLUSION

Edible plant-based scaffolds composed of okara powder, soy protein isolate, sodium alginate, and yerba mate extract were successfully developed and demonstrated significant potential for application in cultivated meat production. The incorporation of okara induced significant structural modifications in the polymeric network, including enhanced microporosity, improved water retention, and greater dimensional stability, resulting in scaffolds with physicochemical and biofunctional properties compatible with the requirements of muscle tissue engineering. In addition, the preservation of functional protein groups and the formation of an interconnected porous architecture favored nutrient diffusion, cellular infiltration, and metabolite exchange, which are critical parameters for efficient three-dimensional cell culture systems.

The developed matrices also exhibited controlled biodegradation and high *in vitro* digestibility, while enabling sustained release of phenolic compounds and maintaining antioxidant activity during simulated gastrointestinal digestion. These characteristics reinforce the multifunctional nature of the scaffolds, combining structural support with potential bioactive functionality, an increasingly desirable feature in next-generation cultivated meat systems. Cell culture assays further demonstrated that scaffolds containing 5% OKP effectively supported the adhesion, proliferation, and spatial distribution of C2C12 cells and bovine myoblasts under static culture conditions, confirming their biocompatibility and suitability as edible support matrices for muscle cell development.

From a sustainability perspective, the valorization of agro-industrial by-products such as okara and yerba mate aligns with current trends in Food Process Engineering and cellular agriculture, which focus on circular bioeconomy strategies, waste reduction, and the development of low-cost, food-grade biomaterials. Overall, the findings highlight the potential of these fully plant-based scaffolds as multifunctional platforms for cultivated-meat applications, while also emphasizing the need for future investigations into dynamic bioreactor cultivation, long-term tissue maturation, mechanical stimulation, and scale-up feasibility to support industrial implementation.

Ethics declarations

Declaration of competing interest

The authors declare that they have no known competing financial interests or personal relationships that could have appeared to influence the work reported in this paper.

Statement on the Use of Generative AI and AI-assisted Technologies

During the preparation of this manuscript, the authors used generative AI tools (ChatGPT, Grammarly, and Gemini) to revise the language, including grammatical and orthographic corrections, clarity improvements, and stylistic enhancements. These tools also provided support in the initial drafting and organization of data presentation. Following the use of these technologies, the authors thoroughly reviewed, validated, and adapted the content. The use of these tools was strictly auxiliary; the intellectual authorship, scientific supervision, and final validation of the entire manuscript remain the sole responsibility of the human authors. The authors confirm that the use of these technologies adhered to the ethical principles of scientific integrity.

Note

This work is part of the Master's thesis of Carlos Henrique Colombo, supervised by Prof. Dr. Kattia Rezzadori.

Acknowledgements

The authors acknowledge the Federal University of Santa Catarina (UFSC) for providing research infrastructure, and the Biotech Network at the Federal University of Santa Catarina (Rede Biotech UFSC) for institutional support and fostering collaborative research.

Funding

This work was supported by the Coordination for the Improvement of Higher Education Personnel (CAPES) (Finance Code 001), the National Institute of Science and Technology in Biofabrics (INCT Biofábricas), and the National Council for Scientific and Technological Development (CNPq) (Grant No. 408414/2024-3). Additional financial support was provided by the Funding Authority for Studies and Projects (FINEP) (Grant No. 2892/22) and the Research and Innovation Support Foundation of the State of Santa Catarina (FAPESC) (Grant Nos. 2024TR001596 and 2024TR002658).

Data Availability

Data will be made available on request.

Competing interests

The authors declare no competing interests.

References

Bach, A. D., Beier, J. P., Stern-Staeter, J., & Horch, R. E. (2004). Skeletal muscle tissue engineering. *Journal of Cellular and Molecular Medicine*, 8(4), 413–422. https://doi.org/10.1111/j.1582-4934.2004.tb00466.x

Bomkamp, C., Skaalure, S. C., Fernando, G. F., Ben-Arye, T., Swartz, E. W., & Specht, E. A. (2022). Scaffolding biomaterials for 3D cultivated meat: Prospects and challenges. *Advanced Science, 9*(3), 2102908. https://doi.org/10.1002/advs.202102908

Burattini, S., Ferri, P., Battistelli, M., Curci, R., Luchetti, F., & Falcieri, E. (2004). C2C12 myoblasts as a model of skeletal muscle development: morpho-functional characterization. *European Journal of Histochemistry*, 48(3), 223–234. https://doi.org/10.4081/893

Chen, X., Zhang, Y., Liu, J., Wang, Y., & Li, H. (2023). Tea polyphenol-coated sodium alginate–gelatin edible scaffold with enhanced properties for cultured meat applications. *Food Hydrocolloids, 145*, 109089. https://doi.org/10.1016/j.foodres.2023.113267

Dai, S., Yao, S., Zhao, J., & Wang, S. (2024). Recent advances in edible scaffolds for cultivated meat: A review. *Trends in Food Science & Technology*, 145, 104380. https://doi.org/10.1016/j.tifs.2024.104380

He, X., Zhao, J., & Cheng, L. (2020). Extraction and characterization of proteins from okara: A byproduct of soybean processing. *Food Chemistry*, 312, 126045. https://doi.org/10.1016/j.foodchem.2019.126045

Li, M., Li, J., Jiao, J., & Wang, S. (2022). Gelatin-soy milk-based scaffolds for skeletal muscle tissue engineering and cultivated meat. *Food Hydrocolloids*, 124, 107224. https://doi.org/10.1016/j.foodhyd.2021.107224

Lim, Y., Suntornnond, R., & Deepak, V. (2024). Scaffold engineering for cultivated meat: Progress and challenges. *Current Opinion in Biotechnology*, 85, 103045. https://doi.org/10.1016/j.copbio.2023.103045

Mariano Jr., E., Lee, D. Y., Lee, J., Choi, Y., Park, J., Han, D., Kim, J. S., Park, J. W., Namkung, S., & Hur, S. J. (2025). A review on the characterization of edible scaffolds for cultured meat: Physical, chemical, biocompatibility, and food safety evaluation methods. *Food Chemistry, 464*, 142493. https://doi.org/10.1016/j.foodchem.2024.142493

Morgado, P. I., Aguiar-Ricardo, A., & Correia, I. J. (2013). Asymmetric membranes as ideal scaffolds for skeletal muscle regeneration. *Polymer International*, 62(5), 701–710. https://doi.org/10.1002/pi.4431

Orellana, N. M., Acevedo, C. A., & Valencia, P. (2020). Scaffolds for cultivated meat: A review on materials and fabrication methods. *Food and Bioprocess Technology*, 13, 201–215. https://doi.org/10.1007/s11947-019-02388-1

Park, S.-M., Ryoo, J.-H., Kwon, H. C., & Han, S. G. (2024). Scaffold biomaterials in the development of cultured meat: A review. *Food Science of Animal Resources, 44*(1), 1–20. https://doi.org/10.5851/kosfa.2023.e74

Pierezan, L., Verruck, S., & Maraschin, M. (2024). Advancements in scaffold design for cultivated meat: The role of plant-based materials. *Innovative Food Science & Emerging Technologies*, 92, 103581. https://doi.org/10.1016/j.ifset.2024.103581

Ravikumar, S., Powell, M., & Huling, J. (2024). Cellular models and regulatory landscapes in cultivated meat production. *Comprehensive Reviews in Food Science and Food Safety*, 23(1), e13289. https://doi.org/10.1111/1541-4337.13289

Robertson, G., Nyman, J., & Suzuki, T. (2024). Proliferation and differentiation of bovine satellite cells on edible biopolymeric films. *Journal of Food Engineering*, 365, 111812. https://doi.org/10.1016/j.jfoodeng.2023.111812

Sabaghi, M., Tavasoli, S., Hoseyni, S. Z., Mozafari, M. R., Degraeve, P., & Katouzian, I. (2022). A critical review on approaches to regulate the release rate of bioactive compounds from biopolymeric matrices. Food Chemistry, 382, 132411. https://doi.org/10.1016/j.foodchem.2022.132411

Santos, D., Silva, F., & Oliveira, J. (2023). Influence of mechanical properties of cellulose acetate scaffolds on C2C12 myoblast behavior. *Polymers*, 15(4), 890. https://doi.org/10.3390/polym15040890

Valenzuela, C., Abugoch, L., & Tapia, C. (2013). Effect of freeze-drying on the properties of protein-based scaffolds. *Journal of Food Science*, 78(8), E1211–E1218. https://doi.org/10.1111/1750-3841.12211

Wong, S. Y. (2010). Composition and functionality of soy okara for food applications. *British Food Journal*, 112(11), 1230–1241. https://doi.org/10.1108/00070701011088196

You, J., Kim, H., & Lee, S. (2025). Polydopamine-coated agarose scaffolds for the expansion of porcine satellite cells in cultivated meat applications. *Food Research International*, 178, 113942. https://doi.org/10.1016/j.foodres.2024.113942

Zhao, X., Liu, L., & Mulvaney, D. R. (2009). Evaluation of myoblast differentiation on unaligned and aligned collagen fibers. *Biotechnology Progress*, 25(1), 244–251. https://doi.org/10.1002/btpr.115

Supplementary Files

This is a list of supplementary files associated with this preprint. Click to download.

- Tables.docx